International Journal of Nanoelectronics and Materials
IJNeaM
ISSN 1985-5761 | E-ISSN 2232-1535

# Synthesis and powder characterization of NiSmCeCu catalysts for the anode reforming layer of solid oxide fuel cells

Saidatul Akmal Biyamin[a,b], Saidatul Haneen Badruhisham[a], Anis Muneerah Shaiful Bahari[a], Nor Anisa Arifin[a], Herma Dina Setiabudi[c], Rogemah Ramli[b], Ng Guat Peng[a], Mohd Eqwan Mohd Roslan[b], Saiful Hasmady Abu Hassan[b], Hassan Mohamed[d*]

[a] *Material Engineering & Testing Group (METG), TNB Research Sdn. Bhd, No. 1, Lorong Ayer Itam, Kawasan Institusi Penyelidikan, 43000 Kajang, Selangor, Malaysia*
[b] *Mechanical Engineering Department, College of Engineering, Universiti Tenaga Nasional (UNITEN), Jalan IKRAM-UNITEN, 43000 Kajang, Selangor, Malaysia*
[c] *Faculty of Chemical & Process Engineering Technology, Universiti Malaysia Pahang Al-Sultan Abdullah, Lebuhraya Tun Razak, 26300 Gambang, Kuantan, Pahang, Malaysia*
[d] *Institute of Sustainable Energy (ISE), Universiti Tenaga Nasional (UNITEN), Jalan IKRAM-UNITEN, 43000 Kajang, Selangor, Malaysia*
∗ *Corresponding author. e-mail: hassan.mohamed@tnb.com.my*

Received 7 July 2025, Revised 20 November 2025, Accepted 18 December 2025

**ABSTRACT**

Solid oxide fuel cells (SOFCs), a type of fuel cell that can operate on several fuels without requiring an external reformer, are among the most promising fuel cell types. However, the effects of hydrocarbon fuels, associated with carbon deposition and poisoning, hinder the performance of solid oxide fuel cells (SOFCs). Conventional anodes of composite nickel-yttria-stabilized zirconia (Ni-YSZ) are not resistant to both, leading to long-term deterioration. One of the strategies to mitigate the impact of carbon deposition and poisoning is to introduce a catalyst reforming layer. The performance of the catalyst reforming layer is associated with the raw materials produced through synthesis methods. Thus, this paper studies three wet synthesis routes for producing powders of catalyst materials, namely sol-gel (SG), solution combustion synthesis (SCS), and co-precipitation (CP). An X-ray diffraction (XRD) analysis reveals that all the synthesis methods successfully formed the NiSmCeCu-based catalysts with different crystallite sizes. The sol-gel method exhibited the smallest crystallite size, approximately 32.7 nm, followed by solution combustion at 39.4 nm and co-precipitation at 49.4 nm. The pore size and Brunauer-Emmett-Teller (BET) surface area of the catalyst from SG also exhibit higher values than those of other methods. The micrograph of the catalyst from SG and SCS reveals a highly porous structure with numerous small cavities. These findings suggest that the SG method offers significant advantages in producing catalyst material with desirable structural and surface characteristics for SOFC application.

**Keywords:** *Wet chemical method, SOFC, hydrocarbon, catalyst, fuel cell*

## 1. INTRODUCTION

Fossil fuel depletion is a critical global issue with profound implications for our current energy generation, environmental sustainability, and future development. For over a century, 80% of the world's energy supply has come from fossil fuels, including coal, oil, and natural gas. However, the finite nature of fossil fuels raises concerns about their long-term availability. Consequently, various renewable energy technologies such as solar, wind, biomass, and hydro have been introduced as alternatives to fossil fuels. Renewable energy can produce green energy, but its sources are intermittent and variable. To stabilize the power output, an energy storage system is necessary, though it may have a limited lifespan and is not environmentally sustainable [1]. On the other hand, a fuel cell is an electrochemical device that converts fuel into electricity without combustion, leading to lower emissions and higher efficiency.

There are several types of fuel cells: alkaline, Proton Exchange Membrane (PEM), Solid Oxide Fuel Cell (SOFC), and Molten Carbonate Fuel Cell (MCFC). Among these, the SOFC is a high-temperature fuel cell that employs dense solid electrolytes, such as yttria-stabilized zirconia. In recent years, SOFC has emerged as a promising technology due to its flexibility, enabling it to utilize various fuels such as hydrocarbons, methane, ammonia, and others [2,3]. The capacity to use diverse fuels expands the potential applications of SOFC from hydrogen to hydrocarbons [4]. However, Ni-based SOFC experiences carbon deposition and coking when using hydrocarbon fuels, as these fuels impair the catalytic activity of Ni, reduce the surface area of the Triple Phase Boundary (TPB), and deteriorate SOFC performance [5–7].

Many studies have been conducted to address these challenges. The strategies can be divided into three: reduction in operating temperature, adjustment of steam ($H_2O$) and carbon (C) ratio, and adding a new anode catalyst [1]. Among these methods, adding new anode catalysts is a promising strategy due to its low cost, simplified system, and variety of materials [2]. Suppressing carbon deposition on the anode can be achieved by depositing a high catalytic activity catalyst layer for hydrocarbon-based fuel over the nickel-based anode [3].

SOFC anode catalyst can be incorporated within the anode, deposited as a separate layer on the anode surface (internal reforming), or independently from the entire cell (external reforming) [1,3,4].

This paper further elaborates on the anode catalyst deposited as a separate layer on the anode surface, referred to as an anode reforming layer. The anode reforming layer converts methane ($CH_4$) and steam ($H_2O$) fuel into carbon monoxide (CO) and carbon (C) before the mixture passes through to the anode, helping to mitigate carbon deposition [3,5]. The discovery of the catalyst layer is primarily attributed to Zhan and Barneet [6]. Zhan and Barneet utilized a ruthenium-supported cerium oxide ($Ru/CeO_2$) as a catalyst layer to enhance the stability of SOFCs by converting an iso-octane/carbon dioxide/steam/air mixture into syngas. Cheng *et al.* employed mesoporous flower-like $Ru/CeO_2$ as a catalyst layer for nickel-based anode, improving cell performance by enhancing the microstructure, as the presence of the catalyst layer hindered the diffusion of fuel gases to the nickel-based anode [7]. With the addition of the catalyst layer, the peak power density of a single cell using $CH_4$ as fuel increased from 297 to 367 mW $cm^{-2}$, representing approximately a 24% improvement [7].

Lois Milner *et al.* have developed a nickel-encapsulated silica ($Ni@SiO_2$) partial oxidation (POX) catalyst to support indirect internal reforming (IRR). The study examines how the silica shell plays a crucial role in preventing catalyst deactivation due to re-oxidation. The findings demonstrate that the silica shell helps maintain the nickel in its reduced state by limiting the rate of oxygen diffusion to the nickel surface. At 750 °C, the catalysts achieved more than 95% methane conversion with high selectivity toward syngas formation [8].

The performance of the catalyst reforming layer depends on the materials used and is also associated with the raw materials produced through various synthesis methods. The chosen synthesis method influences desired properties, such as particle size, specific surface area, and optimal combination of materials. Synthesis methods can be categorized into powder techniques (dry and wet), infiltration, coating, and combination routes [9].

Cesario *et al.* successfully synthesized cobalt-nickel (Co-Ni) and copper-nickel (Cu-Ni) using the Pechini method with high surface area and mitigating carbon deposition for the dry reforming of methane [10]. Bochentyn *et al.* examined praseodymium (Pr) and samarium (Sm) cobalt (Co)-doped ceria (CeO, CeSmO, CePrO, CePrSmO) with several compositions as catalyst layer synthesis by the microemulsion method [11]. This paper finds that Pr-doped ceria exhibits poor adhesion to the Ni-based anode due to a mismatch in the Thermal Expansion Coefficient (TEC). In contrast, Sm and Co doping help reduce the TEC mismatch, improving adhesion [11]. Blaszczak *et al.* evaluate the synthesis of SOCF catalytic material lanthanum strontium cerium nickel titanate (LaSrCeNiTiO), also known as LSCNT, using the Pechini method [3]. This material significantly improves stability and has a higher current density when used with synthetic biogas. Jing Li synthesized the gold/molybdenum disulfide ($Au/MoS_2$) catalyst material by the impregnation method. $Au/MoS_2$ is a promising anode catalyst that prevents CO poisoning of the $MoS_2$ active sites by exhibiting catalytic activity for CO oxidation in the SOFC system [12].

Gonzalo *et al.* use the Solution Combustion Synthesis (SCS) technique to create nickel oxide-gadolinia-doped ceria (NiO-GDC) and nickel oxide-samarium-doped ceria (NiO-SDC) nanocomposites [1]. The nitrate-fuel combustion method was selected due to its high efficiency and relatively low cost when utilizing citric acid as an organic fuel. The NiO-GDC and NiO-SDC disks presented a good porosity and compaction degree [1].

Among them, the powder route (wet method) is the most popular for synthesizing the anode reforming layer, as it is the easiest, simplest, most eco-friendly, and cheapest. The main objective of this paper is to study the wet method of Sol-Gel (SG), Solution combustion synthesis (SCS), and Co-precipitation (CP) for the synthesis of Bi-Metallic materials (NiSmCeCu) for anode catalyst reforming layer. These materials were selected for their characteristics and abilities to reform the hydrocarbon gas while mitigating the impact of carbon deposition [1,10,13-19].

The three wet synthesis methods were compared and analyzed in detail using a thermogravimetric analyzer (TGA) to determine the sintering temperature, X-ray diffraction (XRD) for phase identification, Brunauer–Emmett–Teller (BET) for surface area analysis, field emission scanning electron microscope (FESEM) for microstructural charcterization, and energy dispersive x-ray spectroscopy (EDX) for elemental distribution. Their characteristics are further explained in terms of particle size, porosity, crystallization, and material properties.

## 2. MATERIALS

The NiSmCeCu catalyst was synthesized using three methods: Sol-Gel, Co-Precipitation, and Solution combustion. The reagents used were nickel (II) nitrate hexahydrate ($Ni(NO_3)_2.6H_2O$, purity = 98%), samarium (III) nitrate hexahydrate ($Sm(NO_3)_3.6H_2O$, purity = 99.9%), cerium (III) nitrate hexahydrate ($Ce(NO_3)_3.6H_2O$, purity = 99.5%), copper (III) nitrate hexahydrate ($Cu(NO_3)_3.6H_2O$, purity = 99%), citric acid ($C_6H_8O_7$), glycine ($NH_2CH_2COOH$), sodium hydroxide (NaOH) and ethanol ($C_2H_6O$). The Ni, Sm, and Ce were supplied by Thermoscientific, while Cu was supplied by Merck. The other reagents were supplied by Sigma Aldrich.

## 3. SYNTHESIS METHOD

### 3.1. Sol-Gel (SG)

The Ni, Sm, Ce, and Cu reagents for synthesis using SG were weighed in a 1:1:1:1 molar ratio and sequentially added to 200 mL deionized (DI) water. The amount of DI water was

determined by calculating the molarity ratio of the solutions [1]. The solution was magnetically stirred at 110 rpm until it completely dissolved. Next, citric acid was added as a chelating agent and stirred until fully dissolved. The amount of citric acid was calculated based on the molar ratio of nitrates to citric acid (1:1) [2]. The solution was heated to 80 °C, and the ethanol solution was added dropwise using a pipette until the pH value reached 6. The solution was then continuously stirred at 110 rpm until it transformed into a gel-like consistency, which took approximately 35 - 40 minutes. The gel mixture was dried in an oven at 80 °C for 24 hours. After the gel mixture was converted into powder, it was manually ground using a mortar and pestle. The powder was calcined in a high-temperature furnace for 2 hours at 800 °C. Finally, the calcined powder was ground again to obtain the final catalyst powder. An illustration of the sol-gel synthesis process is shown in Figure 1.

The chemical reaction [2] involved during the SG synthesis is as follows:

$$Ni(NO_3)_2.6H_2O + Sm(NO_3)_3.6H_2O + Ce(NO_3)_3.6H_2O + Cu(NO_3)_2 + 4C_6H_2O_7 + O_2 \rightarrow NiSmCeCuO_4 + 24CO_2 + 24H_2O + 10NO_2 \quad (1)$$

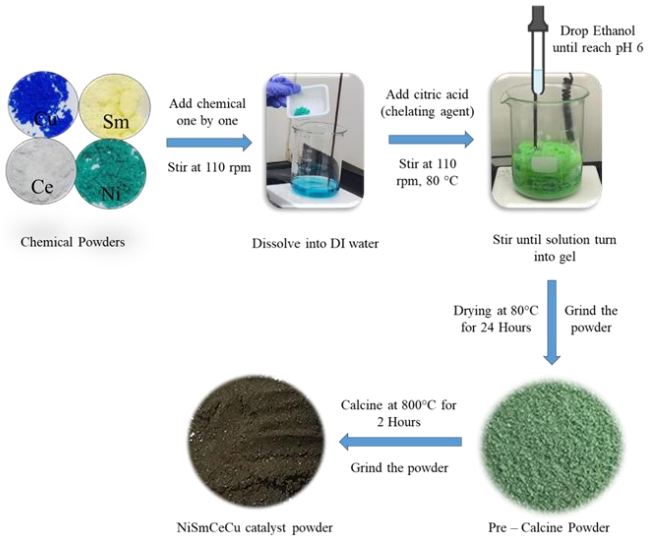


**Figure 1.** Schematic illustration of the Sol-Gel synthesis

### 3.2. Solution combustion synthesis (SCS)

The Ni, Sm, Ce, and Cu reagents for synthesis using SCS were weighed according to the 1:1:1:1 molar ratio and sequentially added to deionized (DI) water. The amount of DI water was determined based on the literature [20]. The solution was magnetically stirred at 110 rpm until it completely dissolved (approximately 40 minutes). Glycine, used as a fuel for the combustion process, was added after the metal nitrates had fully dissolved. The beaker was then covered with aluminum foil, and stirring was continued at 110 rpm for approximately 12 hours.

After 12 hours of stirring, several holes were punctured in the aluminum foil. The magnetic stirrer was removed from the beaker, and a thermocouple was inserted through one of the holes, ensuring it reached the solution without touching the beaker. The temperature of the hot plate was set to 250 °C. The solution began to evaporate and transitioned into a gel-like consistency. Spontaneous combustion occurred at temperatures between 100 °C and 250 °C, with a yellow flame indicating complete combustion.

The combusted powder was collected and then calcined at 800 °C for 2 hours. Finally, the calcined powder was manually ground using a mortar and pestle to obtain the final catalyst powders. An illustration of the combustion solution method is shown in Figure 2

The chemical reaction [21] for SCS is as follows;

$$Ni(NO_3)_2.6H_2O + Sm(NO_3)_3.6H_2O + Ce(NO_3)_3.6H_2O + Cu(NO_3)_2.6H_2O + 5.33NH_2CH_2COOH \rightarrow NiSmCeCuO + 7.67N_2 + 10.66CO_2 + 13.33H_2O \quad (2)$$


**Figure 2.** Schematic illustration of the solution combustion synthesis

### 3.3. Co - Precipitation (CP)

The Ni, Sm, Ce, and Cu reagents for synthesis using CP were weighed in a 1:1:1:1 molar ratio and sequentially added to 25 mL of deionized (DI) water. The amount of DI water was determined based on the stoichiometric molarity ratio of metals [5]. The solution was magnetically stirred at 110 rpm until it was completely dissolved. Simultaneously, 0.1M NaOH solution was prepared as a precipitation agent [5].

The NaOH solution was added to the NiSmCeCu solution and stirred at 110 rpm and 80 °C until fully dissolved, initiating precipitation. This process lasted approximately 2 hours. The solution was then filtered and rinsed several times. The filtered powders were collected in a crucible and dried at 60 °C for 24 hours. After drying, the powders were manually ground using a mortar and pestle, then calcined at 800 °C for 2 hours. Finally, the calcined powders were ground again to obtain the catalyst powders. An illustration of the CP is shown in Figure 3.

The chemical reactions for CP synthesis are as follows;

$$Ni(NO_3)_2.6H_2O + Sm(NO_3)_3.6H_2O + Ce(NO_3)_3.6H_2O + Cu(NO_3)_2.6H_2O + 10NaOH \rightarrow NiSmCeCuO + 10NaNO_3 + 27H_2O \quad (3)$$

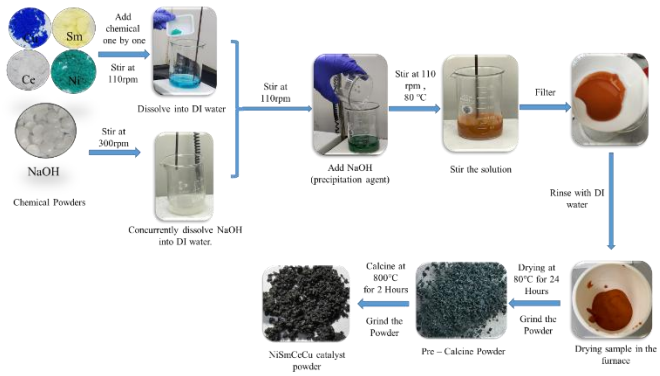


**Figure 3.** Schematic illustration of the Co – Precipitation

### 3.4. Characterization techniques

Before calcination, thermogravimetric analysis (TGA) was performed on the catalyst powder. The analyses for the SG and SCS powders were conducted using a Thermogravimetric Analyzer NETZSCH TG 209 F1 Libra, while the CP powder was analyzed with a Mettler Toledo TGA/DSC 3+. TGA analysis occurred under a nitrogen atmosphere, with the temperature rising from room temperature to 900 °C at a heating rate of 10 °C/min. The calcined powders were examined by X-ray diffractometry (XRD) utilizing a Bruker D8-Advance diffractometer, employing Cu Kα radiation (λ = 1.5406 Å), at room temperature, with a current of 20 mA, a scan step of 0.02°, a scan speed of 3°/min, and an angle range of 2θ = 5°-70°. The crystallite size was estimated using the Scherrer formula. The specific surface area was determined with the Micromeritics 3Flex Adsorption Analyzer, using nitrogen ($N_2$) as the adsorptive gas at -196°C. The samples were degassed for 30 minutes at 150 °C prior to analysis. The morphology of the powder materials was observed using Field Emission Scanning Electron Microscopy (FESEM, Hitachi SU 8020) at an accelerating voltage of 2 kV. The elemental composition and element mapping of the powders were characterized using energy-dispersive spectroscopy (EDS) (Bruker Xflash 6160), which is equipped in the FESEM system.

## 4. RESULTS AND DISCUSSION

### 4.1. Thermogravimetric analysis (TGA)

The pre-calcined powder was subjected to TGA analysis, and the results are recorded in Figure 4. For the SG, initial mass loss occurs around 92.5 °C, with a 7.2% decrease, indicating that the moisture content in the SG is easily removed at low temperature. The subsequent mass loss of 19.0% at around 244.5 °C can be attributed to the decomposition of organic compounds or the removal of chemically bound water. The significant mass loss at around 378.6 °C of 23.0% suggests the decomposition of the primary organic framework or the breakdown of the sol-gel network. Lastly, the final mass loss occurred at approximately 748.5 °C, resulting in a 4.1% decrease. Based on these observations, the suggested calcination temperature for the sol-gel method is between 800 °C and 900 °C. For the SCS, minimal mass change was observed from 0 °C to 800 °C, and significant mass loss began around 800 °C, with a peak at 835.2 °C, suggesting that this temperature range involves substantial changes in the material structure. Thus, a suggested calcination temperature is around 750 °C to 800 °C to ensure calcination without decomposition. In CP, a significant weight loss of 31.1% was recorded at 113.6 °C, attributed to the evaporation of moisture. Subsequently, minimal weight losses were observed at 178.5 °C (2.27%), 221.5 °C (5.63%), and 704.2 °C (4.99%), corresponding to the decomposition of light organic material. Finally, a weight loss of 8.14% occurred at 861.3 °C, suggesting that the calcination temperature of the co-precipitation product is between 800 °C and 900 °C.

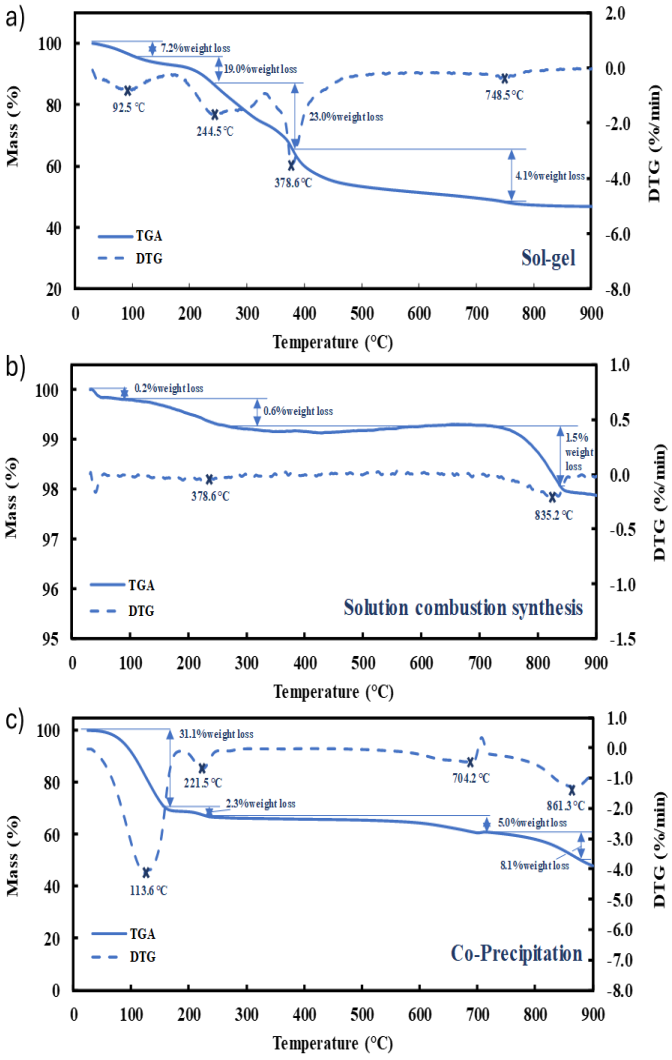


**Figure 4.** Thermal analyses of NiSmCeCu synthesized by a) sol-gel, b) solution combustion synthesis, and c) co-precipitation

With the suggested calcination temperature, the powders for all methods were calcined at 800 °C to further observe their crystallinity, pore size, and morphology. The synthesized powder after the calcination process is shown in Figure 5.

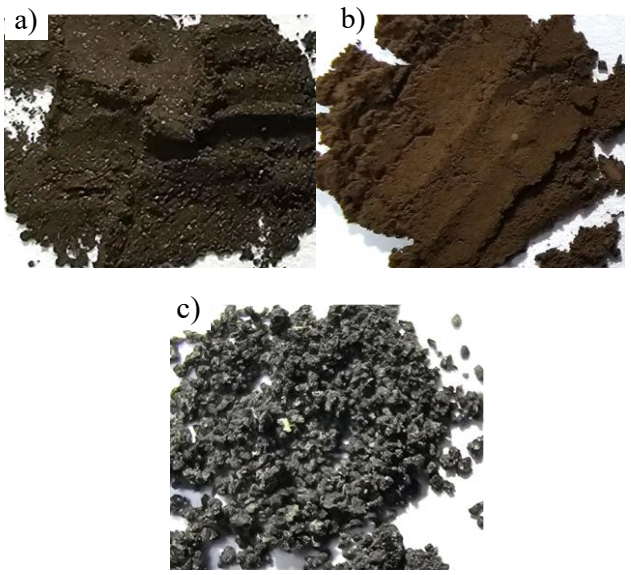


**Figure 5**. Synthesized powder after calcination at 800 °C; a) Sol Gel, b) Solution Combustion Synthesis, c) Co-Precipitation

The preparation of synthesized materials varies based on the method used. The SG method requires additional effort to achieve the consistency necessary to transform a solution into a solid gel phase. In contrast, the SCS method involves a rapid exothermic redox reaction and is more time-efficient compared to the SG and CP methods. However, the filtration and washing steps in the CP method are crucial and demand more time. In terms of ease of preparation, consistency, and repeatability, solution combustion is more time-efficient and reliable than other synthesis methods.

The CP catalyst powder exhibited moisture retention after calcination, as shown in Figure 6, likely due to incomplete removal of NaOH. After several washes, it was suggested that the NaOH had been fully eliminated, resolving the problem as stated in [22,23,24].

**Figure 6.** Water retention of Co-precipitation

### 4.2. X-ray diffraction (XRD)

The X-ray diffraction (XRD) patterns of the powders are shown in Figure 7. The samples are calcined at 800 °C for 2 hours. All the XRD patterns are within the range of 2θ=5°-80°, where SG and SCS exhibited a similar pattern of peak intensity, while the CP has different patterns. The SG and SCS prominent peaks at 2θ = 28.3°, followed by two other peaks at 2θ=32.8°, 47.1°, and 55.9°, respectively. Meanwhile, CP exhibits prominent peaks at 2θ = 31.91°, 36.10°, 53.33°, and 63.50°. The CP exhibited a significantly higher peak intensity compared to SG and SCS. The initial downward trend in the co-precipitation pattern may be attributed to the presence of an amorphous phase and a lower crystallinity phase [10].

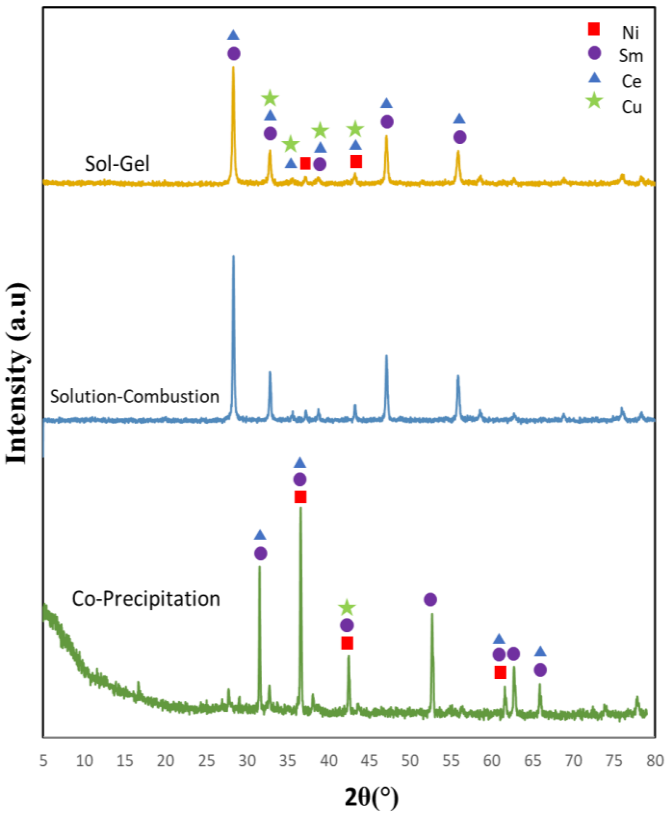


**Figure 7.** XRD pattern of synthesized sol-gel, solution combustion, and co-precipitation

The highest peak for SG and SCS at 2θ=28.3° corresponds to the Joint Committee on Powder Diffraction Standards (JCPDS) 96-154-2110 and 96-152-1461, confirming the successful formation of SmO and CeO, respectively. At 2θ=43.2°, the peak indicates the formation of NiO and CuO (JCPDS 96-432-0491 and 96-721-2234). For the CP, the highest peak at 2θ = 36.10° matches JCPDS 96-432-0509, 96-153-8972, and 96-153-1471, indicating the successful formation of NiO, SmO, and CeO. Additionally, at 2θ = 42.10°, the peaks correspond to the formation of NiO, CuO, and SmO (JCPDS 96-432-0509, 96-153-8972, and 96-901-3017). Therefore, SG, SCS, and CP have succeeded in formulating NiSmCeCu-based catalysts.

In both the SG and SCS, the highest peak is observed at 2θ = 28.5°, corresponding to the (222) crystal plane. This is followed by other peaks at 2θ = 32.8°, 47.1°, and 55.9°, which correspond to the (040), (044), and (262) crystal planes, respectively. In contrast, the CP method shows the highest peak at 2θ = 36.10°, corresponding to the (111) crystal plane, followed by peaks at 2θ = 31.91° and 53.33°, which correspond to the (110) and (233) crystal planes, respectively. All the samples exhibit high crystallinity; however, some CP samples may contain amorphous content, as indicated by the decreasing intensity at lower 2θ values [25]. Furthermore, the different peak position between the CP method with SG and SCS methods may be attributed to differences in synthesis routes, elemental distribution, and concentration of Ni, Sm, Ce, and Cu [26].

**Table 1.** Crystallite size of the samples

| Sample | Crystallite size (nm) |
|---|---|
| Sol-Gel | 32.7 |
| Solution Combustion | 39.4 |
| Co-Precipitation | 49.4 |

**4.3.**

### 4.4. Brunauer-Emmett-Teller (BET)

Figure 8 presents the $N_2$ adsorption-desorption isotherms for NiSmCeCu catalysts synthesized using the SG, SCS, and CP, with the insets showing the pore size distributions for each method. This analysis highlights the significant impact of synthesis methods on pore characteristics, surface area, and pore structure.

The adsorption isotherm of NiSmCeCu synthesized via the SG exhibits a gradual increase in adsorption followed by a sharp rise at high relative pressures, suggesting mesoporous characteristics, which align with the pore size distribution graph. The hysteresis loop indicates capillary condensation, typically Type IV. In contrast, the isotherms for catalysts synthesized by SCS and CP display a sharp increase at high $P/P_o$, suggesting mesopore or macropore structures. The pore distribution graph shows the meso-to-macroporous range. The presence of a hysteresis loop with steep adsorption at high relative pressures suggests Type V.

Table 2 summarizes the BET surface area, pore volume, and average pore diameter of NiSmCeCu synthesized using SG, SCS, and CP. As shown in Table 2, the average pore size and BET surface area of the NiSmCeCu synthesized via SG are ca. 3.3 nm and 336.9 $m^2/g$, respectively. This finding confirms the presence of mesopores, indicating that the SG synthesis produces a material with a higher surface area and a well-developed mesoporous structure [28]. In contrast, with an average pore size exceeding 140 nm, NiSmCeCu synthesized via SCS and CP suggests a highly macroporous structure, where adsorption occurs primarily at high relative pressures ($P/P_0 > 0.9$). The sharp increase in adsorption near saturation confirms the prevalence of large macropores.

**Table 2.** BET surface area, pore volume, and average pore diameter of NiSmCeCu synthesized using SG, SCS, and CP

| Sample | BET Surface Area ($m^2/g$) | Pore Volume ($cm^3/g$) | Average Pore Diameter (nm) |
|---|---|---|---|
| Sol-gel | 336.9 | 0.554 | 3.3 |
| Solution combustion | 2.3 | 0.162 | 142.1 |
| Co-precipitation | 0.9 | 0.121 | 269.9 |

The large gaps in average pore diameter between NiSmCeCu catalysts synthesized using SG, SCS, and CP are mostly due to fundamental differences in their synthesis methods. The SG method creates the smallest pores (~3.3 nm) by regulated hydrolysis and condensation processes, resulting in a homogeneous gel network at the molecular level [29]. Following drying and calcination, this network may transform into well-connected mesopores, resulting in a narrow and controllable pore size distribution [9]. The SCS method produces bigger pores (~142.1 nm), which may be due to its quick and exothermic reaction that generates enormous amounts of gas in a short time [30]. This may produce foaming and structural expansion, which results in loosely packed frameworks with macropores. The CP method results in the highest average pore size (~269.9 nm), which may be attributed to uncontrolled nucleation and development, followed by particle agglomeration during drying and sintering [9]. Thus, the substantial variance in pore size is directly related to how each approach influences the development and evolution of the porous network.

The BET surface areas and pore volumes follow the order: SG > SGS > CP. The higher nitrogen adsorption by the SG sample suggests a greater surface area and potentially more active sites, which can enhance its catalytic performance [31,32]. Meanwhile, the macroporous samples synthesized via SCS and CP exhibit lower adsorption capacities, which may result in lower surface areas, potentially impacting their catalytic efficiency.

The SG method had a better performance, which may be due to its ability to produce catalysts with a large surface area, a homogeneous mesoporous structure, and well-connected pore networks [9,29]. Unlike SCS and CP, which frequently produce irregular macropores and reduced surface areas due to fast or uncontrolled processes, the SG approach enables molecular-level mixing and regulated hydrolysis-condensation reactions [29]. The Type IV isotherm and narrow pore size distribution (~3.3 nm) support the creation of a more homogeneous gel with well-distributed, smaller pores. These structural advantages improve gas accessibility and expose more active sites,

making SG-synthesized NiSmCeCu a better choice for catalytic applications [9,29,33]. However, the SG method is sensitive to small changes in synthesis factors such as pH, solvent ratios, and precursor concentrations [9,33]. Small variations in these circumstances can have a considerable impact on gelation behavior and reproducibility, particularly when utilizing different metal precursors with varied reactivity [9].

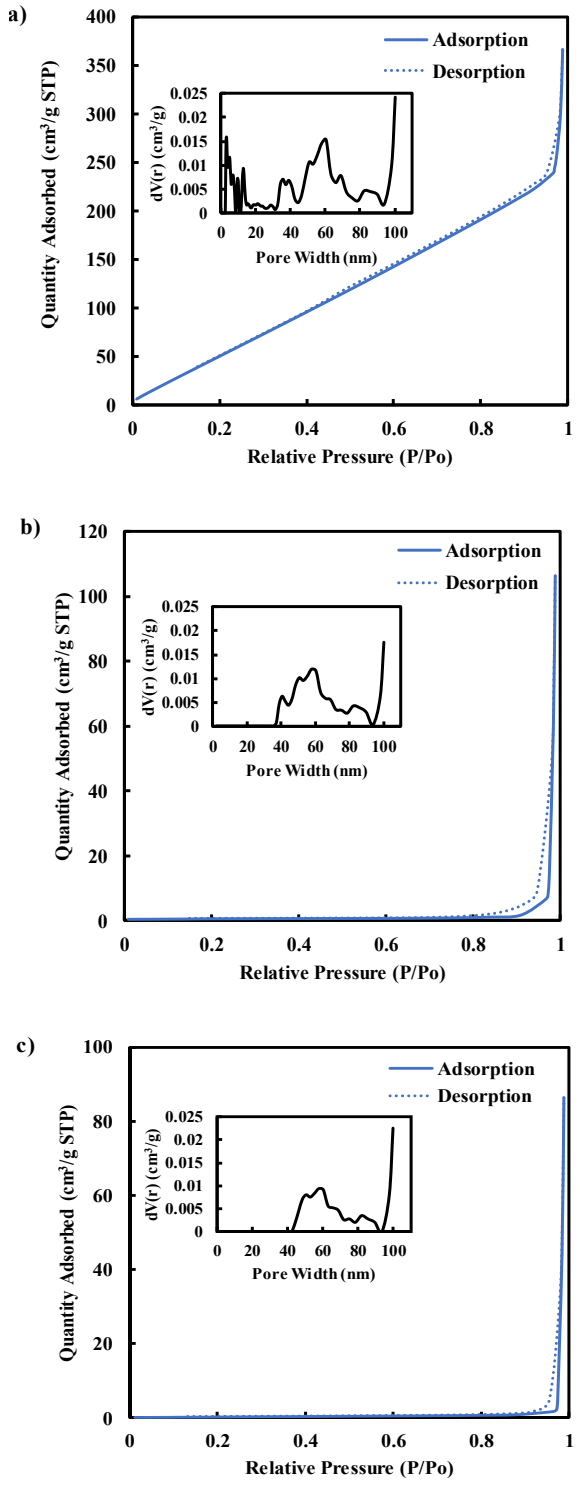


**Figure 8.** $N_2$ adsorption isotherm and pore size distribution (inset) of NiSmCeCu synthesized by a) sol-gel (SG), b) solution combustion synthesis (SCS), and c) co-precipitation (CP)

### 4.5. Field Emission Scanning Electron Microscopy (FESEM) & Energy Dispersive Spectroscopy (EDS)

The calcined powder of SG, SGS, and CP was further investigated using FESEM. The micrograph of NiSmCeCu powder for SG, SCS, and CP is shown in Figures 9 – 11. The SG and SCS powders reveal a highly porous structure with numerous small cavities. In contrast, the surface morphology of CP is highly dense and covered with an oxide layer. High porosity is required for the anode reforming layer to be able to break down the hydrocarbon to syngas and allow the penetration of the syngas to other layers [34].

Dispersive X-ray Spectroscopy (EDS) elemental mappings of NiSmCeCu powder, illustrating the distribution of Ni, Sm, Ce, and Cu elements, as shown in Figure 12. The elemental is evenly distributed for SG and SCS. However, for the CP, the elemental is not evenly distributed for the Ni element, suggesting that the powder is not fully homogeneous.

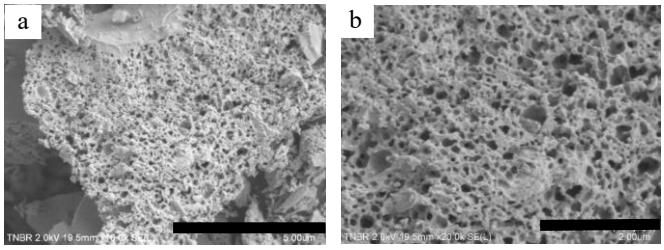


**Figure 9.** Micrograph of SG, a) mag 10K, and b) magnified view of a) at 20K

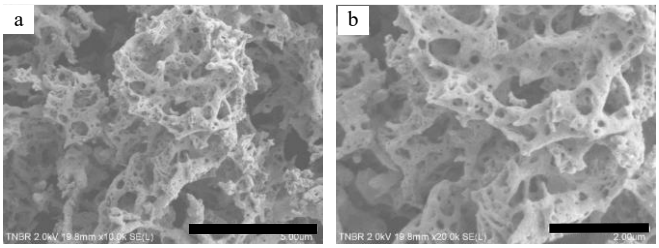


**Figure 10.** Micrograph of SCS, a) mag 10K, and b) magnified view of a) at 20K

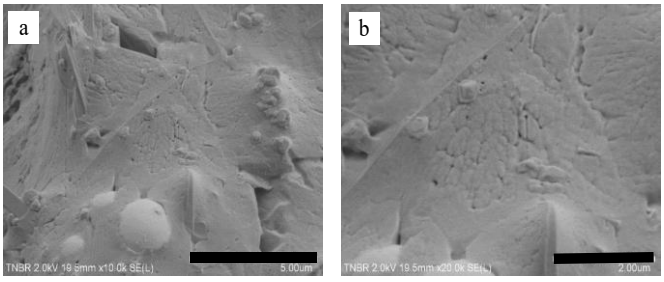


**Figure 11.** Micrograph of CP, a) mag 10K, and b) magnified view of a) at 20K

Table 3 summarizes the EDS elemental percentage for each material (Ni, Sm, Ce, Cu, O) synthesized using different methods. The accelerating voltage used for SG and SCS was 15 kV, while the CP required a higher voltage of 20 kV due

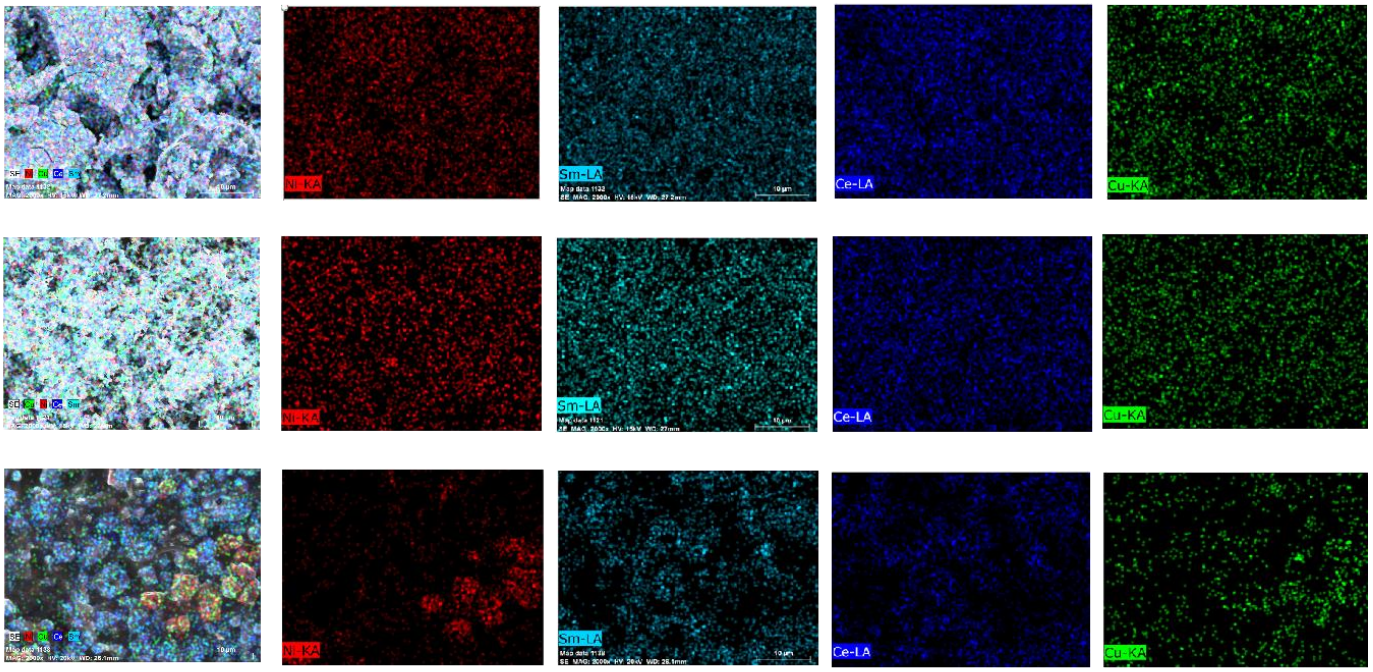


**Figure 12.** EDS mapping of SG, SCS, and CP

to a lower count per second. The analysis was performed at three different spots, and the results were averaged.

**Table 3.** EDS elemental percentage for each material (Ni, Sm, Ce, Cu, O) synthesized using different methods

| Sample | Ni (%) | Sm (%) | Ce (%) | Cu (%) | O (%) |
|---|---|---|---|---|---|
| Sol-gel | 7.88 | 36.96 | 33.45 | 8.04 | 13.64 |
| Solution combustion synthesis | 8.10 | 32.02 | 31.73 | 13.22 | 14.93 |
| Co-precipitation | 3.45 | 26.34 | 24.27 | 2.53 | 43.01 |

The elemental composition of the synthesized powders using SG and SCS shows a similar range when compared to the CP. The oxide (O) percentage in CP powders is the highest among the three methods, confirming the presence of an oxide layer as indicated in the micrograph in Figure 11. This suggests that the synthesis using SG and SCS does not significantly affect the elemental composition of the materials used.

## 5. CONCLUSION

The SG, SCS, and CP synthesis methods were successfully employed to synthesize NiSmCeCu powder, intended for use as an anode reforming layer in SOFC. The catalyst powder synthesized using the SG method demonstrated superior performance in terms of smaller crystalline size, higher pore volume, and higher surface area. In addition, the powder using the SG method displays a Type IV isotherm, characteristic of mesoporous materials, supported by a narrow pore size distribution of approximately 3.3 nm. The micrograph of NiSmCeCu powder synthesized via SG reveals a notably porous structure when compared to the SCS and CP methods. On the contrary, the SCS and CP samples exhibit Type V isotherms and macroporous structures, with significantly lower surface areas and wider pore size distributions exceeding 140 nm and 260 nm, respectively. In summary, the performance of the synthesis method follows the order: SG > SCS > CP. These findings suggest that the SG method offers substantial benefits in producing catalyst material with desirable structural and surface characteristics for SOFC applications.

## ACKNOWLEDGMENTS

The authors would like to acknowledge the financial support provided by TNB Research Sdn. Bhd.

## REFERENCES

[1] G. Abarzúa, S. Roa, N. Julve-Pérez, and R. V. Mangalaraja, "Solution combustion-based synthesis of NiO-GDC and NiO-SDC nanocomposites for low-temperature SOFC," Ceram. Int., vol. 50, no. 9, pp. 16689–16697, 2024, doi: 10.1016/j.ceramint.2024.02.087.

[2] K. Cai, S Luo, "Sol-gel synthesis of nano block-like ZnMn2O4 using citric acid complexing agent and electrochemical performance as anode for lithium-ion batteries," J. Alloys Compd., vol. 909, p. 164882, 2022, doi: 10.1016/j.jallcom.2022.164882.

[3] P. Błaszczak, M. Łapiński, S. F. Wang, P. Jasiński, and B. Bochentyn, "Exsolution of Ni nanoparticles on the surface of cerium and nickel co-doped lanthanum strontium titanate as a new anodic layer for DIR-SOFC. Anti-coking potential and H2S poisoning resistance of the prepared material," Int. J. Hydrogen

Energy, vol. 45, no. 53, pp. 29186–29200, 2020, doi: 10.1016/j.ijhydene.2020.07.162.

[4] P. Zhang Z.Yang, Y.Jin, C. Liu, Z.Lei, F. Chen and S.Peng "Progress report on the catalyst layers for hydrocarbon-fueled SOFCs," Int. J. Hydrogen Energy, vol. 46, no. 79, pp. 39369–39386, 2021, doi: 10.1016/j.ijhydene.2021.09.198.

[5] Y. Zhang Z.Yang D.Yin, Y.Liu, C.Fei, R.Xiong, J,Shi and G.Yan "Composition and magnetic properties of cobalt ferrite nano-particles prepared by the co-precipitation method," J. Magn. Magn. Mater., vol. 322, no. 21, pp. 3470–3475, 2010, doi: 10.1016/j.jmmm.2010.06.047.

[6] Z. Zhan and S. A. Barnett, "An Octane-Fueled Solid Oxide Fuel Cell," vol. 95, no. March, 2005.

[7] Z. Cheng, W. Zhang, J. Wei, Y. Mao, and C. Sun, "Ni and Ru bimetal nanoparticles-anchored porous Mo2C nanorods used as an internal reforming catalyst layer for hydrocarbon-fueled solid oxide fuel cells," Int. J. Hydrogen Energy, vol. 62, no. February, pp. 140–147, 2024, doi: 10.1016/j.ijhydene.2024.03.054.

[8] L. Milner-Elkharouf, M. Khzouz, and R. Steinberger-Wilckens, "Catalyst development for indirect internal reforming (IIR) of methane by partial oxidation," Int. J. Hydrogen Energy, vol. 45, no. 8, pp. 5285–5296, 2020, doi: 10.1016/j.ijhydene.2019.05.026.

[9] S. H. Badruhisham, A. M. Shaiful Bahari, S. A. Biyamin, N. A. Arifin, and N. G. Peng, "Wet Chemical Synthesis of Anode Reforming Layer in Solid Oxide Fuel Cell: A Comprehensive Review of Sol-Gel, Co-Precipitation and Combustion Synthesis," Int. J. Nanoelectron. Mater., vol. 17, no. 3, pp. 363–379, 2024, doi: 10.58915/ijneam.v17i3.1113.

[10] M. R. Cesario, G.Souza, F. Loureiro, A. Araujo, J. Grilo, S. Aroud, H. Tidahy, D. Macedo, D. Fagg, C. Gennequin and E. Abi-Aad "Synthesis of Co–Ni and Cu–Ni based-catalysts for dry reforming of methane as potential components for SOFC anodes," Ceram. Int., vol. 47, no. 23, pp. 33191–33201, 2021, doi: 10.1016/j.ceramint.2021.08.220.

[11] B. Bochentyn, P. Błaszczak, M. Gazda, A. Fuerte, and S. Wang, "ScienceDirect Investigation of praseodymium and samarium co- doped ceria as an anode catalyst for DIR-SOFC fueled by biogas," vol. 5, pp. 0–11, 2020, doi: 10.1016/j.ijhydene.2020.07.146.

[12] Z. R. Xu, J. L. Luo, and K. T. Chuang, "The study of Au/MoS2 anode catalyst for solid oxide fuel cell (SOFC) using H2S-containing syngas fuel," J. Power Sources, vol. 188, no. 2, pp. 458–462, 2009, doi: 10.1016/j.jpowsour.2008.12.008.

[13] B. Bochentyn, M. Chlipała, M. Gazda, S. F. Wang, and P. Jasiński, "Copper and cobalt co-doped ceria as an anode catalyst for DIR-SOFCs fueled by biogas," Solid State Ionics, vol. 330, no. August 2018, pp. 47–53, 2019, doi: 10.1016/j.ssi.2018.12.007.

[14] A. Mizera, P. Błaszczak, B. Bochentyn, R. Lach, and E. Drożdż, "Cu supported on various oxides as a candidate catalyst for dry methane reforming in DIR-SOFCs systems," Int. J. Hydrogen Energy, vol. 47, no. 61, pp. 25647–25661, 2022, doi: 10.1016/j.ijhydene.2022.06.016.

[15] Y. Liu, Z. Shao, T. Mori, and S. P. Jiang, "Development of nickel based cermet anode materials in solid oxide fuel cells – Now and future," Mater. Reports Energy, vol. 1, no. 1, p. 100003, 2021,
doi: 10.1016/j.matre.2020.11.002.

[16] Z. Wang, Y. Wang, D. Qin, Y.Gu, H.Yu, B.Qian and Y.Chao "Improving electrochemical performance of (Cu, Sm)CeO2 anode with anchored Cu nanoparticles for direct utilization of natural gas in solid oxide fuel cells," J. Eur. Ceram. Soc., vol. 42, no. 7, pp. 3254–3263, 2022, doi: 10.1016/j.jeurceramsoc.2022.02.006.

[17] M. Choolaei, E. Jakubczyk, and B. Amini Horri, "Synthesis and characterisation of a ceria-based cobalt-zinc anode nanocomposite for low-temperature solid oxide fuel cells (LT-SOFCs)," Electrochim. Acta, vol. 445, no. November 2021, p. 142057, 2023,
doi: 10.1016/j.electacta.2023.142057.

[18] A. C. Chien, N. J. Ye, C. W. Huang, and I. H. Tseng, "Studies of nickel/samarium-doped ceria for catalytic partial oxidation of methane and effect of oxygen vacancy," Catalysts, vol. 11, no. 6, pp. 1–12, 2021, doi: 10.3390/catal11060731.

[19] A. Fuerte, R. X. Valenzuela, M. J. Escudero, and L. Daza, "Study of a SOFC with a bimetallic Cu-Co-ceria anode directly fuelled with simulated biogas mixtures," Int. J. Hydrogen Energy, vol. 39, no. 8, pp. 4060–4066, 2014, doi: 10.1016/j.ijhydene.2013.06.142.

[20] S. Hajarpour, A. Honarbakhsh Raouf, and K. Gheisari, "Structural evolution and magnetic properties of nanocrystalline magnesium-zinc soft ferrites synthesized by glycine-nitrate combustion process," J. Magn. Magn. Mater., vol. 363, pp. 21–25, 2014,
doi: 10.1016/j.jmmm.2014.03.027.

[21] M. Agthe, "Rare Earth Oxide Nanopowder (RE = Nd, Eu, Gd, Ho, Y, Yb) by Combustion Synthesis, Sulfation and Calcination : Role of the Initial Structure," Rare Earth Oxide Nanopowder, 2011,

[22] J. H. Kang, Y. M. Kim, H. S. Kim, M. S. Lee, J. H. Jang, and J. H. Jo, "Fabrication characteristics of SOFC single cell using nanocrystalline 1Ce10ScSZ electrolyte powder prepared by co-precipitation process," J. Fuel Cell Sci. Technol., vol. 9, no. 1, pp. 1–6, 2012, doi: 10.1115/1.4003783.

[23] L. Spiridigliozzi, G. Dell'Agli, A.Marocco, G.Accardo, M.Pansimi, S.P. Yoon, H.C Ham and D. Frattini "Engineered co-precipitation chemistry with ammonium carbonate for scalable synthesis and sintering of improved Sm0.2Ce0.8O1.90 and Gd0.16Pr0.04Ce0.8O1.90 electrolytes for IT-SOFCs," J. Ind. Eng. Chem., vol. 59, no. February, pp. 17–27, 2018, doi: 10.1016/j.jiec.2017.10.001.

[24] T. L. Gilbile, R. S. Pawar, V. N. Kapatkar, R. C. Kamble, and S. S. Pawar, "Synthesis and Performance Tuning

of Sm 0.2 Ce 0.8 O 2−δ Electrolyte for Low Temperature Solid Oxide Fuel Cell Application," J. Electron. Mater., vol. 48, no. 6, pp. 4117–4124, 2019, doi: 10.1007/s11664-019-07184-9.

[25] A. Rajaeiyan and M. M. Bagheri-Mohagheghi, "Comparison of sol-gel and co-precipitation methods on the structural properties and phase transformation of γ and α-Al2O3 nanoparticles," Adv. Manuf., vol. 1, no. 2, pp. 176–182, 2013, doi: 10.1007/s40436-013-0018-1.

[26] K. Ploner, P. Delir Kheyrollahi Nezhad, A. Gili, F. Kamatzki, A. Gurlo, A. Doran, P. Cao, M. Heggen, N. Kowitsch, M. Armbruster, M. Watschinger, B.Klotzer and S. Penner "The sol-gel autocombustion as a route towards highly CO2-selective, active and long-term stable Cu/ZrO2methanol steam reforming catalysts," Mater. Chem. Front., vol. 5, no. 13, pp. 5093–5105, 2021, doi: 10.1039/d1qm00641j.

[27] Z. Li, M. Peng, X. Zhang, L. Zhang, J. Li, and Y. Sun, "Preparation of SOFC Anodes at Lower Temperature with Boosted Electrochemical Performance," ACS Appl. Energy Mater., vol. 6, no. 6, pp. 3616–3626, 2023, doi: 10.1021/acsaem.3c00278.

[28] A. Matsumoto, H. Misran, and K. Tsutsumi, "Adsorption characteristics of organosilica based mesoporous materials," Langmuir, vol. 20, no. 17, pp. 7139–7145, 2004, doi: 10.1021/la0360409.

[29] Y. Han and L. Zhang, "Synthesis of Mesoporous Silica Using the Sol – Gel Approach : Adjusting Architecture and Composition for Novel Applications," 2024.

[30] H. Cheng, S. Chen, L. Jang, and H. Liu, "Glycine – Nitrate Combustion Synthesis and Photocatalytic Degradation Properties of Cu-Based Nanoparticles," no. December, 2019.

[31] C. Wang, X. Liu, J. P. Chen, and K. Li, "Superior removal of arsenic from water with zirconium metal-organic framework UiO-66," Sci. Rep., vol. 5, pp. 1–10, 2015, doi: 10.1038/srep16613.

[32] A.M. Shaiful Bahari, N.A. Amin, M.Z.A Zulkifli, A.N Alias, N. Rosli, S.A. Sazali, N. Abu Hasan, Z. Lockman, Z.Amin Nowshad, H.Misran "Facile Synthesis of Chloride-less Zirconium-based Metal- Organic Framework (MOF) as Chromium (VI) Removal via Photoreduction," vol. 17, no. 2, pp. 220–238, 2021.

[33] A. M. Shaiful Bahari, S.Z. Othman, M.F. Mohamad Fadli, M.Z.A Zulkifli, S.A. Biyamin, M.A.A Islam, Z.Amin, Nowshad, H.Misran "Facile synthesis of Zr-based metal-organic gel (Zr-MOG) using 'green' sol-gel approach," Surfaces and Interfaces, vol. 27, no. December 2020, p. 101469, 2021, doi: 10.1016/j.surfin.2021.101469.

[34] M. F. Rabuni, T. Li, M. H. D. Othman, F. H. Adnan, and K. Li, "Progress in Solid Oxide Fuel Cells with Hydrocarbon Fuels," Energies, vol. 16, no. 17, pp. 1–36, 2023, doi: 10.3390/en16176404.